



SOFIA/HAWC+ View of an Extremely Luminous Infrared Galaxy: WISE 1013+6112

Yoshiki Toba^{1,2,3} , Wei-Hao Wang² , Tohru Nagao³ , Yoshihiro Ueda¹ , Junko Ueda⁴, Chen-Fatt Lim^{2,5} ,
Yu-Yen Chang² , Toshiki Saito⁶ , and Ryohei Kawabe^{4,7,8}

¹ Department of Astronomy, Kyoto University, Kitashirakawa-Oiwake-cho, Sakyo-ku, Kyoto 606-8502, Japan; toba@kusastro.kyoto-u.ac.jp

² Academia Sinica Institute of Astronomy and Astrophysics, 11F of Astronomy-Mathematics Building, AS/NTU, No.1, Section 4, Roosevelt Road, Taipei 10617, Taiwan

³ Research Center for Space and Cosmic Evolution, Ehime University, 2-5 Bunkyo-cho, Matsuyama, Ehime 790-8577, Japan

⁴ National Astronomical Observatory of Japan, 2-21-1 Osawa, Mitaka, Tokyo, 181-8588, Japan

⁵ Graduate Institute of Astrophysics, National Taiwan University, P.O. Box 23-141, Taipei 10617, Taiwan

⁶ Max Planck Institute for Astronomy, Königstuhl 17, D-69117 Heidelberg, Germany

⁷ Department of Astronomy, The University of Tokyo, 7-3-1 Hongo, Bunkyo-ku, Tokyo 113-0033, Japan

⁸ Department of Astronomical Science, Graduate University for Advanced Studies (SOKENDAI), 2-21-1 Osawa, Mitaka, Tokyo 181-8588, Japan

Received 2019 October 9; revised 2019 December 9; accepted 2019 December 11; published 2020 January 28

Abstract

We present far-infrared (FIR) properties of an extremely luminous infrared galaxy (ELIRG) at $z_{\text{spec}} = 3.703$, WISE J101326.25+611220.1 (WISE 1013+6112). This ELIRG is selected as an IR-bright dust-obscured galaxy based on the photometry from the Sloan Digital Sky Survey and the *Wide-field Infrared Survey Explorer* (WISE). In order to derive its accurate IR luminosity, we perform follow-up observations at 89 and 154 μm using the High-resolution Airborne Wideband Camera-plus (HAWC+) on board the 2.7 m Stratospheric Observatory For Infrared Astronomy (SOFIA) telescope. We conduct spectral energy distribution (SED) fitting with CIGALE using 15 photometric data (0.4–1300 μm). We successfully pin down FIR SED of WISE 1013+6112 and its IR luminosity is estimated to be $L_{\text{IR}} = (1.62 \pm 0.08) \times 10^{14} L_{\odot}$, making it one of the most luminous IR galaxies in the universe. We determine the dust temperature of WISE 1013+6112 is $T_{\text{dust}} = 89 \pm 3$ K, which is significantly higher than that of other populations such as submillimeter galaxies and FIR-selected galaxies at similar IR luminosities. The resultant dust mass is $M_{\text{dust}} = (2.2 \pm 0.1) \times 10^8 M_{\odot}$. This indicates that WISE 1013+6112 has a significant active galactic nucleus and star-forming activity behind a large amount of dust.

Unified Astronomy Thesaurus concepts: Active galaxies (17); Infrared galaxies (790); Quasars (1319); Supermassive black holes (1663)

1. Introduction

Galaxies whose infrared (IR) luminosity exceeds 10^{13} and $10^{14} L_{\odot}$ have been termed as hyper-luminous IR galaxies (HyLIRGs; Rowan-Robinson 2000) and extremely luminous IR galaxies (ELIRGs; Tsai et al. 2015), respectively. Their IR luminosity (L_{IR}) is expected to be produced by star formation (SF), active galactic nucleus (AGN) activity, or both. In the context of major merger scenario, their extreme IR luminosity could indicate that it corresponds to the peak of AGN and/or SF activity behind a large amount of gas and dust (Narayanan et al. 2010; Ricci et al. 2017; Blecha et al. 2018). Therefore, it is important to search for IR luminous galaxies such as HyLIRGs and ELIRGs to understand the galaxy formation and evolution and connection to their supermassive black holes (see, e.g., Hopkins et al. 2008). However, their volume densities are extremely low (Rowan-Robinson & Wang 2010; Gruppioni et al. 2013), and thus wide and deep surveys are required to detect these spatially rare populations.

One successful technique to search for HyLIRGs and ELIRGs is based on mid-IR (MIR) colors taken with the *Wide-field Infrared Survey Explorer* (WISE; Wright et al. 2010). Most objects that are faint or undetected by WISE at 3.4 μm (W1) and 4.6 μm (W2) but are well detected at 12 μm (W3) or 22 μm (W4) are classified as HyLIRGs/ELIRGs. They are termed hot dust-obscured galaxies (DOGs⁹) or “W1W2

dropouts” (Eisenhardt et al. 2012; Wu et al. 2012). Indeed, a hot DOG with $L_{\text{IR}} = 2.2 \times 10^{14} L_{\odot}$ was reported as the most luminous galaxy in the universe (Tsai et al. 2015). However, Fan et al. (2018) recently reported that this ELIRG is contaminated by a foreground galaxy, resulting in an overestimation of its total IR luminosity by a factor of about two (see also Tsai et al. 2018).

Toba & Nagao (2016) also performed an extensive search for HyLIRGs and ELIRGs using the Sloan Digital Sky Survey (SDSS; York et al. 2000) and WISE. By combining the SDSS Data Release 12 (DR12; Alam et al. 2015) spectroscopic catalog and ALLWISE catalog (Cutri et al. 2014), they selected optically-faint but IR bright objects with $i - [22] > 7.0$ and flux density at 22 $\mu\text{m} > 3.8$ mJy in 14,555 deg², where i and [22] are i -band and 22 μm AB magnitudes, respectively, yielding 67 objects with spectroscopic redshift. These objects are known as IR-bright DOGs (Toba et al. 2015, 2017c; Noboriguchi et al. 2019). Toba & Nagao (2016) then estimated their tentative IR luminosities based on the spectral energy distribution (SED) fitting with a SED fitting code. SED Analysis using Bayesian Statistics (SEABASS; Rovilos et al. 2014) (see also Toba et al. 2017a), where they used only SDSS and WISE data (see Figure 6 in Toba & Nagao 2016). Consequently, an IR-bright DOG, WISE J101326.25+611220.1 (hereafter WISE 1013+6112) at spectroscopic redshift ($z_{\text{spec}} = 3.70$) was left as an ELIRG candidate.

Toba et al. (2018) then executed follow-up observations of WISE 1013+6112 with the Submillimetre Common User Bolometer Array 2 (SCUBA-2; Holland et al. 2013) on the

⁹ The original definition of DOGs was flux density at 24 $\mu\text{m} > 0.3$ mJy and $R - [24] > 14$, where R and [24] represent Vega magnitudes in the R -band and 24 μm , respectively (see Dey et al. 2008, for more detail).

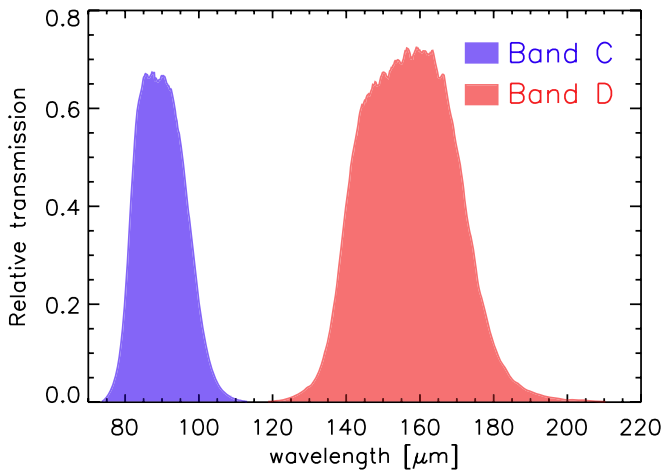


Figure 1. HAWC+ filter transmission profiles for bands C (blue) and D (red).

James Clerk Maxwell telescope (JCMT) (S17AP002, PI: Y. Toba), and the Submillimeter Array (SMA: Ho et al. 2004) (2016BA003, PI: Y. Toba). They performed the SED fitting by adding data points at 450 and 850 μm (SCUBA-2/JCMT) and 870 and 1300 μm (SMA), and discussed the possibility of beaming and lensing amplification. The derived IR luminosity was $L_{\text{IR}} = 2.2^{+1.5}_{-1.0} \times 10^{14} L_{\odot}$, making it an ELIRG. However, as we did not have deep rest-frame MIR and far-IR (FIR) photometry responsible for FIR SED, the derived IR luminosity remains a large uncertainty. In order to constrain the IR luminosity of this ELIRG more accurately and to investigate the SF activity and dust properties of its host galaxy, we require deep FIR data.

In this paper, we present follow-up observations of an extremely luminous DOG, WISE 1013+6112, at 89 and 154 μm using a High-resolution Airborne Wideband Camera-plus (HAWC+: Harper et al. 2018) on the 2.7 m Stratospheric Observatory for Infrared Astronomy (SOFIA) telescope (Temi et al. 2018). These observations with HAWC+/SOFIA enable us to pin down the FIR SED of WISE 1013+6112. Throughout this paper, the adopted cosmology is a flat universe with $H_0 = 70 \text{ km s}^{-1} \text{ Mpc}^{-1}$, $\Omega_M = 0.3$, and $\Omega_{\Lambda} = 0.7$, which are same as those adopted in Toba et al. (2018). Solar luminosity is defined as $L_{\odot} = 3.828 \times 10^{33} \text{ erg s}^{-1}$ (Mamajek et al. 2015).

2. Data and Analysis

2.1. Follow-up Observations with SOFIA

Flux densities at 89 and 154 μm were obtained using HAWC+/SOFIA in Cycle 6 (PI: Y. Toba). The filter transmission profiles¹⁰ for these bands are shown in Figure 1. Data have been obtained for the observation (PlanID: 06_0029) during HAWC+ mission 2019-02-13_HA_F546. We performed the total intensity mapping with HAWC+ bands C (89 μm) and D (154 μm) providing angular resolutions of $7''.8$ and $13''.6$ in FWHM, respectively. The total on-source integration times were approximately 100 minutes at both 89 and 154 μm . Data were reduced using the HAWCDPR PIPELINE v1.3.0 (Harper et al. 2018). As the source is faint, these data are processed using the faint option.

Figure 2 shows the FIR image of WISE 1013+6112 taken by HAWC+. WISE 1013+6112 was marginally detected at 89 μm with a signal-to-noise ratio (S/N) = 4.1, while this object was clearly detected at 154 μm with S/N = 9.8 that was evaluated using 2D Gaussian fitting (see below). The flux measurements were performed with the same approach used for SCUBA-2 and SMA data in Toba et al. (2018). We employed the Common Astronomy Software Applications (CASA) package (ver. 5.5.0; McMullin et al. 2007). We performed a 2D Gaussian fit for each image and estimated the total fluxes within $10'' \times 10''$ and $20'' \times 20''$ apertures, respectively. The photometry of WISE 1013+6112, including SOFIA FIR flux densities measured in this work, is summarized in Table 1.

2.2. SED Fitting with CIGALE

We employed the Code Investigating Galaxy Emission (CIGALE¹¹; Burgarella et al. 2005; Noll et al. 2009; Boquien et al. 2019) to conduct a detailed SED modeling in a self-consistent framework by considering the energy balance between the ultraviolet/optical and IR. In this code, users can handle various parameters, such as star formation history (SFH), single stellar population (SSP), attenuation law, AGN emission, dust emission, and radio synchrotron emission (see, e.g., Toba et al. 2019a, 2019b, 2020).

SFH is assumed as two exponential decreasing star formation rates (SFRs) with different e-folding times (Ciesla et al. 2015, 2016), where we parameterized the e-folding time of the main stellar population (τ_{main}) and the late starburst population (τ_{burst}), mass fraction of the late burst population (f_{burst}), and age of the main stellar population in the galaxy (see Section 3.1.2 in Boquien et al. 2019, for details). We used the stellar templates provided from Bruzual & Charlot (2003) assuming the Chabrier (2003) initial mass function (IMF), and the standard default nebular emission model included in CIGALE (see Inoue 2011). Dust attenuation is modeled using the Calzetti et al. (2000) starburst attenuation curve with a small Magellanic cloud (SMC) extinction curve (Pei 1992), where the color excess of the emission lines $E(B - V)_{\text{lines}}$ is parameterized. The color excess of stars, $E(B - V)_{*}$ can be converted from $E(B - V)_{\text{lines}}$ by assuming a simple reduction factor ($f_{\text{EBV}} = \frac{E(B - V)_{*}}{E(B - V)_{\text{lines}}} = 0.44$ (Calzetti 1997). For AGN emission, we utilized models provided by Fritz et al. (2006). In order to avoid a degeneracy of AGN templates in the same manner as in Ciesla et al. (2015) and Toba et al. (2019b), we fixed certain parameters that determine the density distribution of the dust within the torus, i.e., ratio of the maximum-to-minimum radii of the dust torus ($R_{\text{max}}/R_{\text{min}}$), optical depth at 9.7 μm ($\tau_{9.7}$), density profile along the radial and the polar distance coordinates parameterized by β and γ (see Equation (3) in Fritz et al. 2006), and opening angle (θ). Hence, we parameterized the ψ parameter (an angle between equatorial axis and line of sight) that corresponds to a viewing angle of the torus. We further parameterized the AGN fraction (f_{AGN}) that is the contribution of IR luminosity from the AGN to the total IR luminosity (Ciesla et al. 2015).

Since one of the purposes of this work is to derive the dust temperature (T_{dust}), we employed the analytic model provided by Casey (2012) for dust emission. This model consists of two components: one is a single temperature modified blackbody (MBB) and the other is power-law emission in the MIR. As the MIR power-law component is expected to be dominated by the

¹⁰ <https://www.sofia.usra.edu/science/proposing-and-observing/observers-handbook-cycle-8/7-hawc/71-specifications#FiltersHAWC>

¹¹ <https://cigale.lam.fr/2018/11/07/version-2018-0/>

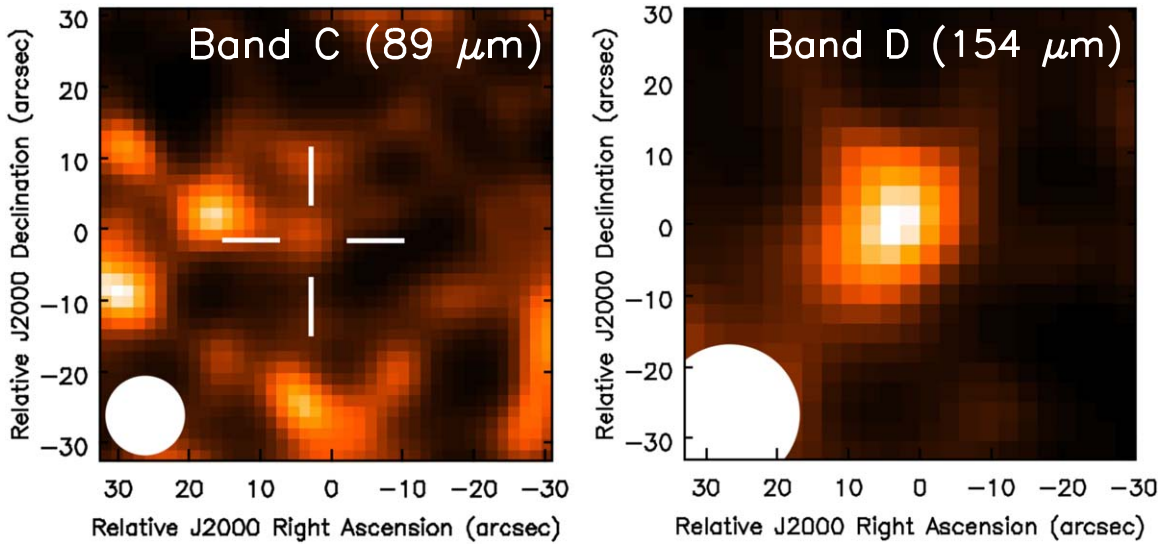


Figure 2. Total flux images at 89 μm (left) and 154 μm (right). Relative coordinates in units of arcsec with respect to the SDSS position of WISE 1013+6112 are employed. The white filled circles are beam sizes for each band. The object considered here in the left panel is located at the center of the white cross.

Table 1
Observed Properties of WISE 1013+6112

| | |
|--|----------------------------------|
| WISE J101326.25+611220.1 | |
| R.A. (SDSS) (J2000.0) | 10:13:26.24 |
| Decl. (SDSS) (J2000.0) | +61:12:19.76 |
| Redshift (SDSS) | 3.703 ± 0.001 |
| SDSS <i>u</i> -band (μJy) | $< 1.26^a$ |
| SDSS <i>g</i> -band (μJy) | 3.47 ± 0.47 |
| SDSS <i>r</i> -band (μJy) | 13.70 ± 0.67 |
| SDSS <i>i</i> -band (μJy) | 13.58 ± 0.95 |
| SDSS <i>z</i> -band (μJy) | 21.09 ± 4.03 |
| WISE 3.4 μm (mJy) | 0.05 ± 0.01 |
| WISE 4.6 μm (mJy) | 0.13 ± 0.01 |
| WISE 12 μm (mJy) | 3.30 ± 0.16 |
| WISE 22 μm (mJy) | 10.70 ± 0.98 |
| HAWC+/SOFIA 89 μm (mJy) | 22.5 ± 5.5 |
| HAWC+/SOFIA 154 μm (mJy) | 63.4 ± 6.5 |
| SCUBA-2/JCMT 450 μm (mJy) | 46.00 ± 8.05^b |
| SCUBA-2/JCMT 850 μm (mJy) | 13.35 ± 0.67^b |
| SMA 870 μm (mJy) | 13.60 ± 2.72^b |
| SMA 1.3 mm (mJy) | 6.49 ± 1.30^b |
| $L_{\text{IR}} (L_{\odot})$ | $(1.62 \pm 0.08) \times 10^{14}$ |
| $L_{\text{IR}}^{\text{AGN}} (L_{\odot})$ | $(1.13 \pm 0.06) \times 10^{14}$ |
| $L_{\text{IR}}^{\text{SF}} (L_{\odot})$ | $(0.49 \pm 0.10) \times 10^{14}$ |
| $M_{*} (M_{\odot})$ | $(2.03 \pm 0.36) \times 10^{11}$ |
| SFR ($M_{\odot} \text{ yr}^{-1}$) | $(2.81 \pm 0.36) \times 10^3$ |
| $T_{\text{dust}} (\text{K})$ | $(8.9 \pm 0.3) \times 10$ |
| $M_{\text{dust}} (M_{\odot})$ | $(2.2 \pm 0.1) \times 10^8$ |

Notes.

^a 3σ upper limit.

^b See Toba et al. (2018) for details.

AGN torus emission that was already taken into account in Fritz et al. (2006) model, we focus only on the MBB component. MBB is formulated as $1 - e^{-\tau(\nu)} \nu^{\beta} B_{\nu}(T_{\text{dust}})$, where ν is the frequency, β is the emissivity index of the dust, and $B_{\nu}(T_{\text{dust}})$ is the Planck function. $\tau \equiv (\nu/\nu_0)^{\beta}$ is the optical depth, where ν_0 is the frequency where optical depth equals unity (Draine 2006). In this work, we fixed $\nu_0 = 1.5 \text{ THz}$ ($\lambda_0 = 200 \mu\text{m}$) (e.g., Conley et al. 2011) and $\beta = 1.6$ (e.g., Fan et al. 2016), and parameterized

only T_{dust} . We confirmed that the choice of ν_0 and β does not significantly affect the following results as long as $\nu_0 < 1.5 \text{ THz}$ and $\beta = 1-2$ are adopted (see also Kovács et al. 2006). Note that the Casey (2012) model does not include polycyclic aromatic hydrocarbon (PAH) emission that could dominate MIR emission (particularly for SF galaxies), in exchange for parameterizing dust temperature. However, we confirmed that the resultant IR luminosity is consistent with what we reported in this work even when we used other dust models with PAH emission such as the one by Dale et al. (2014). The detailed parameter ranges adopted in the SED fitting are tabulated in Table 2.

3. Results and Discussions

3.1. IR Luminosity

Figure 3 shows the SED of WISE 1013+6112 in the rest frame at $z_{\text{spec}} = 3.70$. The observed data points of WISE 1013+6112 are well fit by the combination of stellar, AGN, and SF components with an adequately reduced χ^2 ($=0.67$). The resultant IR luminosity is $L_{\text{IR}} = (1.62 \pm 0.08) \times 10^{14} L_{\odot}$, which is consistent with the value reported in Toba et al. (2018) ($L_{\text{IR}} = 2.2_{-1.0}^{+1.5} \times 10^{14} L_{\odot}$) within the errors. Nevertheless, we have successfully estimated IR luminosity more accurately owing to additional FIR data taken by HAWC+/SOFIA; the relative error of L_{IR} was reduced approximately to 5%. We confirmed that WISE 1013+6112 is still one of the most IR luminous galaxies in the universe.

The AGN fraction defined as $L_{\text{IR}}(\text{AGN})/L_{\text{IR}}$ is 0.7, which is smaller than what was reported in Toba et al. (2018) ($f_{\text{AGN}} = 0.9_{-0.20}^{+0.06}$). This is because Toba et al. (2018) overestimated AGN luminosity owing to the lack of SOFIA data that covered the peak of the FIR luminosity. We found that WISE 1013+6112 is still AGN-dominated but SF luminosity moderately contributes to the total IR luminosity (see Section 3.2).

3.2. Host Properties

We discuss host properties, stellar mass (M_{*}) and SFR, of WISE 1013+6112 in this subsection. The resultant M_{*} and SFR outputs by CIGALE are $M_{*} = (2.03 \pm 0.36) \times 10^{11} M_{\odot}$

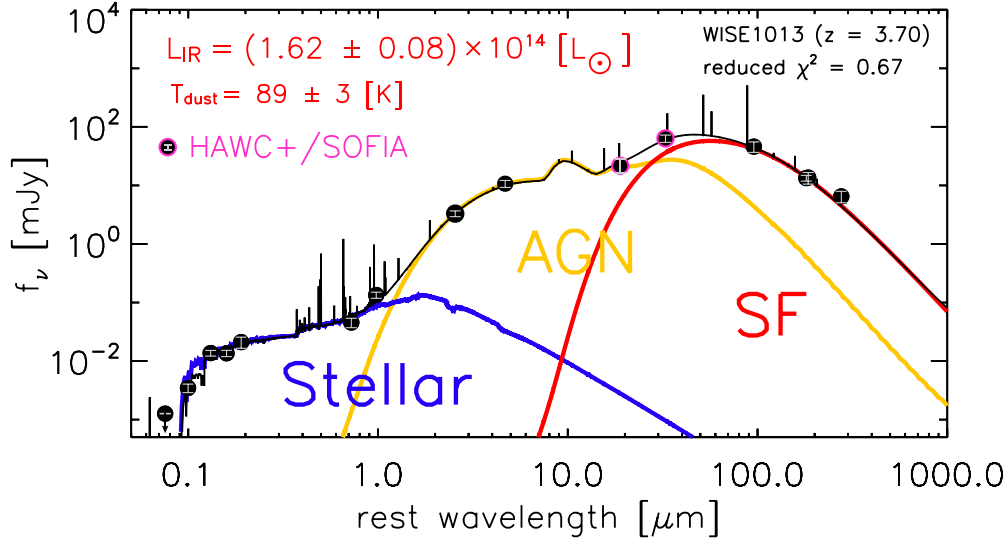


Figure 3. SED of WISE 1013+6112. The black points are photometric data, two of which are new data obtained in this work (black and magenta circles). The contribution from the stellar, AGN, and SF components to the total SED are shown as blue, yellow, and red lines, respectively. The black solid line represents the resultant best-fit SED.

Table 2
Parameter Ranges Used in the SED Fitting with CIGALE

| Parameter | Value |
|---------------------------------|---|
| | Double exp. SFH |
| τ_{main} (Myr) | 50, 100, 500, 1000, 3000 |
| τ_{burst} (Myr) | 3, 5, 8, 10 |
| f_{burst} | 0.5, 0.7, 0.8, 0.9, 0.95 |
| age (Myr) | 500, 1000, 3000, 5000 |
| | SSP (Bruzual & Charlot 2003) |
| IMF | Chabrier (2003) |
| Metallicity | 0.02 |
| | Dust Attenuation (Calzetti et al. 2000) |
| $E(B - V)_{\text{lines}}$ | 0.2, 0.4, 0.6, 0.8, 1.0 |
| f_{EBV} | 0.44 |
| Extinction curve | SMC (Pei 1992) |
| | AGN Emission (Fritz et al. 2006) |
| $R_{\text{max}}/R_{\text{min}}$ | 150 |
| $\tau_{9.7}$ | 0.6 |
| β | 0.00 |
| γ | 0.0 |
| θ | 60 |
| ψ | 0.001, 60.100, 89.990 |
| f_{AGN} | 0.1, 0.2, 0.3, 0.4, 0.5, 0.6, 0.7, 0.8, 0.9 |
| | Dust Emission (Casey 2012) |
| T_{dust} (K) | 10, 20, 30, 40, 50, 60, 70, 80, 90, 100 |
| Emissivity β | 1.6 |

and $\text{SFR} = (2.81 \pm 0.36) \times 10^3 M_{\odot} \text{ yr}^{-1}$, respectively. The stellar mass is in good agreement with that reported in Toba et al. (2018). On the other hand, SFR is 2.2 times larger than that reported in Toba et al. (2018). This is reasonable because Toba et al. (2018) underestimated the SF luminosity as discussed in Section 3.1, and SFR derived here is more reliable with small uncertainty. We confirmed that WISE 1013+6112 shows a significant offset with respect to the main-sequence

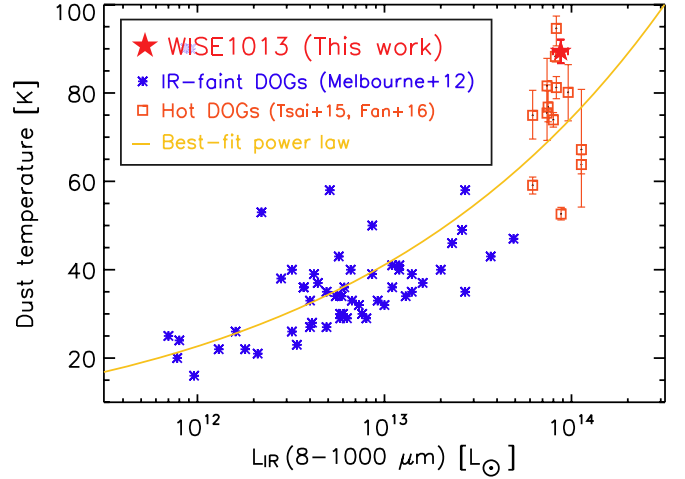


Figure 4. Dust temperature as a function of IR luminosity, L_{IR} (8–1000 μm). The blue asterisks represent IR-faint DOGs (Melbourne et al. 2012), while the orange squares represent hot DOGs (Tsai et al. 2015; Fan et al. 2016). The red star represents WISE 1013+6112. The yellow line is the best-fit power law for all data points, with $T_{\text{dust}} = 0.02 \times L_{\text{IR}}^{0.26}$.

galaxies at $3 < z < 4$ (Tomczak et al. 2016). Given the same stellar mass, the SFR of WISE 1013+6112 is roughly an order of magnitude higher than that of SF galaxies at similar redshifts, suggesting that WISE 1013+6112 still has very active SF. The resultant SFH, i.e., $(\tau_{\text{main}}, \tau_{\text{burst}}, f_{\text{burst}}, \text{age}) = (100 \text{ Myr}, 10 \text{ Myr}, 0.95, 1000 \text{ Myr})$ suggests that WISE 1013+6112 might have an instantaneous starburst that lasts a few hundred million years.

3.3. Dust Temperature

We then discuss the dust temperature (T_{dust}) heated by SF activity in WISE 1013+6112. Although Toba et al. (2018) discussed T_{dust} qualitatively based on the ratio of flux densities at the observed frame between 850 and 22 μm , our data set covering around the peak of FIR emission from dust enables us to do more quantitative discussion.

The dust temperature derived by the SED fitting is $T_{\text{dust}} = 89 \pm 3$ K. This temperature is significantly higher than that of submillimeter galaxies (SMGs; Chapman et al. 2005; Kovács et al. 2006) and that of FIR-selected HyLIRGs (Yang et al. 2007), whose T_{dust} ranges from 30 to 60 K. This result is consistent with what was reported qualitatively in Toba et al. (2018).

This high dust temperature was also reported in a nearby ultraluminous IR galaxy (ULIRG), Arp 220 at $z = 0.018$ (Wilson et al. 2014); the estimated T_{dust} of the eastern part in Arp 220 is about 80 K. The IR luminosity surface density of WISE 1013+6112 (with an effective radius of ~ 2 kpc) is about $10^{12} L_{\odot} \text{ kpc}^{-2}$, which is roughly consistent with that of eastern “nucleus (0.08 kpc \times 0.12 kpc)” of Arp 220 (Wilson et al. 2014). This result could suggest that WISE 1013+6112 has extreme activity that is comparable to the nucleus activity of nearby ULIRGs, over the galaxy scale.

Figure 4 shows dust temperature as a function of IR luminosity for various DOG populations: IR-faint DOGs at $0.82 < z < 4.41$ (Melbourne et al. 2012) whose MIR flux densities are fainter than those of IR-bright DOGs, hot DOGs at $1.68 < z < 4.59$ (Tsai et al. 2015; Fan et al. 2016), and WISE 1013+6112 at $z = 3.70$. We note that the definition of IR luminosity is often different in the literature. Historically, IR luminosity is defined as luminosity integrated over a wavelength range of 8–1000 μm (e.g., Sanders & Mirabel 1996; Chary & Elbaz 2001), which allows stellar emissions to contribute toward the IR luminosity. On the other hand, recent SED fitting codes such as CIGALE and Multiwavelength Analysis of Galaxy Physical Properties (MAGPHYS; da Cunha et al. 2008, 2015) employ physically-motivated IR luminosity without any boundary for the integration range in wavelength. The IR luminosity is defined as the energy re-emitted by dust that absorbs radiations from stellar and AGNs (see Boquien et al. 2019). In order to compare IR luminosity with the literature under the same conditions, we integrated the best-fit SED to estimate L_{IR} (8–1000 μm) to be $9.0 \times 10^{13} L_{\odot}$, which is plotted in Figure 4.

The dust temperature of IR-faint DOGs in Melbourne et al. (2012) is 20–60 K, which is consistent with other studies of IR-faint DOGs (Calanog et al. 2013). We found that there is a correlation between T_{dust} and L_{IR} (8–1000 μm), with $T_{\text{dust}} = 0.02 \times L_{\text{IR}}^{0.26}$, and WISE 1013+6112 is located at the luminous end of the correlation. The $T_{\text{dust}}-L_{\text{IR}}$ correlation for IR galaxies was reported by several authors (e.g., Dunne et al. 2000; Chapman et al. 2003; Amblard et al. 2010; Hwang et al. 2010; Magnelli et al. 2014; Liang et al. 2019), although the origin of this correlation is still under debate (see Schreiber et al. 2018, and references therein). One possibility is that as (i) the dust temperature is also likely to depend on redshift (e.g., Magdis et al. 2012; Béthermin et al. 2015; Genzel et al. 2015) and (ii) those DOGs plotted in Figure 4 are flux-limited samples (i.e., IR luminosity correlates with redshift), the observed $T_{\text{dust}}-L_{\text{IR}}$ correlation might be due to the selection effect.

Note that WISE 1013+6112, with a flux density at $3.4 \mu\text{m} > 50 \mu\text{Jy}$ does not satisfy the selection criteria of hot DOGs¹² whose flux density at $3.4 \mu\text{m}$ must be smaller than

$34 \mu\text{Jy}$ (Eisenhardt et al. 2012). The name “hot” DOGs originates from the fact that the dust temperature of hot DOGs is much hotter than that of IR-faint, classical DOGs (see Dey et al. 2008), which is consistent with the trend seen in Figure 4. This result could suggest that once IR luminosity exceeds $10^{14} L_{\odot}$, i.e., in an ELIRG regime, MIR-selected objects may have a high dust temperature regardless of satisfying the hot DOG criteria.

3.4. Dust Mass

Finally, we derive the dust mass (M_{dust}) of WISE 1013+6112 with the same method as Toba et al. (2017b), where M_{dust} is derived from the following formula:

$$M_{\text{dust}} = \frac{D_L^2}{1+z} \frac{S(\nu_{\text{obs}})}{\kappa_{\text{rest}} B(\nu_{\text{rest}}, T_{\text{dust}})}, \quad (1)$$

where $S(\nu_{\text{obs}})$ is flux density at observed frequency (ν_{obs}), D_L is the luminosity distance, κ_{rest} is the dust mass absorption coefficient at rest frequency (ν_{rest}), and $B(\nu_{\text{rest}}, T_{\text{dust}})$ is the Planck function at temperature T_{dust} and at ν_{rest} . We estimated dust mass at $850 \mu\text{m}$ ($\nu_{\text{rest}} = 353$ GHz) using a dust absorption coefficient of $\kappa(850 \mu\text{m}) = 0.383 \text{ cm}^2 \text{ g}^{-1}$ (Draine 2003) and the $T_{\text{dust}} = 89$ K (see Section 3.3). Here we employed the Monte Carlo technique to calculate the dust mass and its uncertainty. Assuming a Gaussian distribution with a mean (T_{dust}) and sigma (its uncertainty), we randomly chose one value among the distributions as an adopted T_{dust} . We repeated this process 10,000 times and calculated the mean and standard deviation of the resultant M_{dust} distribution. The estimated dust mass is $M_{\text{dust}} = (2.1 \pm 0.1) \times 10^8 M_{\odot}$. The estimated dust-to-stellar mass ratio of WISE 1013+6112 is $\log(M_{\text{dust}}/M_{\star}) = -2.96$, which is roughly consistent with that of star-forming galaxies at $z > 2.5$ (Santini et al. 2014; Calura et al. 2017).

We found that the resultant dust mass of WISE 1013+6112 is inconsistent with what is expected from the $M_{\text{dust}}-\text{SFR}$ relation for local galaxies at $z < 0.3$ (da Cunha et al. 2010); extrapolating the relation to high SFR shows that the observed dust mass is about two orders of magnitude smaller than predicted (see also Lianou et al. 2019). This would indicate that the $M_{\text{dust}}-\text{SFR}$ relation depends on the redshift. This discrepancy was also reported by Hjorth et al. (2014), who mentioned that a difference in evolutionary sequence causes galaxies to move around in the diagram and contributes to the scatter of the $M_{\text{dust}}-\text{SFR}$ relation. Indeed, given a high SFR, the dust mass of dusty starburst galaxies at $z \sim 2-4$ tends to have a smaller dust mass compared to local SDSS galaxies (Swinbank et al. 2014). The dust mass of those high- z starburst galaxies is roughly consistent with that of WISE 1013+6112. Nevertheless, in order to explain such a large dust mass of WISE 1013+6112 at $z = 3.7$, an efficient and rapid dust formation process may be required (Hjorth et al. 2014).

4. Summary and Conclusions

In this paper, we report FIR properties of an extremely luminous DOG (WISE 1013+6112) at $z_{\text{spec}} = 3.703$. Thanks to the multiwavelength data set of the SDSS, WISE, SOFIA, SCUBA-2, and SMA, we pinned down their SEDs at rest frames of 0.1–300 μm . In particular, adding the observed-frame 89 and 154 μm data taken by HAWC+ is crucial to constrain the peak of the FIR SED. We derived physical quantities of

¹² The exact criteria for hot DOGs are $W1 > 17.4$ ($< 34 \mu\text{Jy}$), and either (i) $W4 < 7.7$ (> 6.9 mJy) and $W2-W4 > 8.2$ or (ii) $W3 < 10.6$ (> 1.7 mJy) and $W2-W3 > 5.3$, where $W1$, $W2$, $W3$, and $W4$ are given in Vega magnitude (Eisenhardt et al. 2012).

WISE 1013+6112 such as IR luminosity and dust temperature based on the SED fitting with CIGALE. The resultant IR luminosity is $L_{\text{IR}} = (1.62 \pm 0.08) \times 10^{14} L_{\odot}$, making it one of the most luminous IR galaxies in the universe. The derived dust temperature is $T_{\text{dust}} = 89 \pm 3$ K, which is significantly higher than that of other populations such as SMGs and FIR-selected galaxies. We observed that there exists a positive correlation between the L_{IR} and T_{dust} of DOGs, including classical IR-faint DOGs and hot DOGs, with $T_{\text{dust}} = 0.02 \times L_{\text{IR}}^{0.26}$, and WISE 1013+6112 is located at the luminous end of this correlation. The dust mass inferred from T_{dust} is $M_{\text{dust}} = (2.1 \pm 0.1) \times 10^8 M_{\odot}$, which is inconsistent with what is expected from the $M_{\text{dust}}\text{-SFR}$ relation for local galaxies. Efficient formation of dust from the metals may need to be considered to produce such a high dust mass, given the redshift of $z = 3.7$.

We gratefully acknowledge the anonymous referee for a careful reading of the manuscript and very helpful comments. We are deeply thankful to Drs. Lopez-Rodrigue Enrique and Ralph Y. Shuping for helping with the observations and data analysis taken by HAWC+/SOFIA. We also thank Prof. Denis Burgarella for helping us to understand CIGALE code.

This work is based [in part] on observations made with the NASA/DLR Stratospheric Observatory for Infrared Astronomy (SOFIA). SOFIA is jointly operated by the Universities Space Research Association, Inc. (USRA), under NASA contract NNA17BF53C, and the Deutsches SOFIA Institut (DSI) under DLR contract 50 OK 0901 to the University of Stuttgart.

The Submillimeter Array is a joint project between the Smithsonian Astrophysical Observatory and the Academia Sinica Institute of Astronomy and Astrophysics and is funded by the Smithsonian Institution and the Academia Sinica.

The James Clerk Maxwell Telescope has historically been operated by the Joint Astronomy Centre on behalf of the Science and Technology Facilities Council of the United Kingdom, the National Research Council of Canada and the Netherlands Organisation for Scientific Research. Additional funds for the construction of SCUBA-2 were provided by the Canada Foundation for Innovation. Funding for SDSS-III has been provided by the Alfred P. Sloan Foundation, the Participating Institutions, the National Science Foundation, and the U.S. Department of Energy Office of Science. The SDSS-III website is <http://www.sdss3.org/>.

SDSS-III is managed by the Astrophysical Research Consortium for the Participating Institutions of the SDSS-III Collaboration including the University of Arizona, the Brazilian Participation Group, Brookhaven National Laboratory, Carnegie Mellon University, University of Florida, the French Participation Group, the German Participation Group, Harvard University, the Instituto de Astrofísica de Canarias, the Michigan State/Notre Dame/JINA Participation Group, Johns Hopkins University, Lawrence Berkeley National Laboratory, Max Planck Institute for Astrophysics, Max Planck Institute for Extraterrestrial Physics, New Mexico State University, New York University, the Ohio State University, Pennsylvania State University, University of Portsmouth, Princeton University, the Spanish Participation Group, University of Tokyo, University of Utah, Vanderbilt University, University of Virginia, University of Washington, and Yale University.

This publication makes use of data products from the *Wide-field Infrared Survey Explorer*, which is a joint project of the

University of California, Los Angeles, and the Jet Propulsion Laboratory/California Institute of Technology, funded by the National Aeronautics and Space Administration.

This work is supported by JSPS KAKENHI grants No. 18J01050 and 19K14759 (Y. Toba), 16H03958, 17H01114, and 19H00697 (T. Nagao), and 17K05384 (Y. Ueda). Y. Toba and W.H.W. acknowledge the support from the Ministry of Science and Technology of Taiwan (MOST 105-2112-M-001-029-MY3 and MOST 108-2112-M-001-014-).

Facilities: SOFIA (HAWC+), Sloan, WISE, SMA, JCMT.

Software: IDL, IDL Astronomy User's Library (Landsman 1993), CASA (v5.5.0) (McMullin et al. 2007), CIGALE (Boquien et al. 2019).

ORCID iDs

Yoshiki Toba  <https://orcid.org/0000-0002-3531-7863>
 Wei-Hao Wang  <https://orcid.org/0000-0003-2588-1265>
 Tohru Nagao  <https://orcid.org/0000-0002-7402-5441>
 Yoshihiro Ueda  <https://orcid.org/0000-0001-7821-6715>
 Chen-Fatt Lim  <https://orcid.org/0000-0003-1213-9360>
 Yu-Yen Chang  <https://orcid.org/0000-0002-6720-8047>
 Toshiki Saito  <https://orcid.org/0000-0002-2501-9328>
 Ryohei Kawabe  <https://orcid.org/0000-0002-8049-7525>

References

- Alam, S., Albareti, F. D., Allende Prieto, C., et al. 2015, *ApJS*, 219, 12
 Amblard, A., Cooray, A., Serra, P., et al. 2010, *A&A*, 518, L9
 Béthermin, M., Daddi, E., Magdis, G., et al. 2015, *A&A*, 573, A113
 Blecha, L., Snyder, G. F., Satyapal, S., & Ellison, S. L. 2018, *MNRAS*, 478, 3056
 Boquien, M., Burgarella, D., Roehly, Y., et al. 2019, *A&A*, 622, A103
 Bruzual, G., & Charlot, S. 2003, *MNRAS*, 344, 1000
 Burgarella, D., Buat, V., & Iglesias-Páramo, J. 2005, *MNRAS*, 360, 1413
 Calanog, J. A., Wardlow, J., Fu, H., et al. 2013, *ApJ*, 775, 61
 Calura, F., Pozzi, F., Cresci, G., et al. 2017, *MNRAS*, 465, 54
 Calzetti, D. 1997, in AIP Conf. Ser. 408, The Ultraviolet Universe at Low and High Redshift, ed. W. H. Waller (Melville, NY: AIP), 403
 Calzetti, D., Armus, L., Bohlin, R. C., et al. 2000, *ApJ*, 533, 682
 Casey, C. M. 2012, *MNRAS*, 425, 3094
 Chabrier, G. 2003, *PASP*, 115, 763
 Chapman, S. C., Blain, A. W., Smail, I., & Ivison, R. J. 2005, *ApJ*, 622, 772
 Chapman, S. C., Helou, G., Lewis, G. F., & Dale, D. A. 2003, *ApJ*, 588, 186
 Chary, R., & Elbaz, D. 2001, *ApJ*, 556, 562
 Ciesla, L., Boselli, A., Elbaz, D., et al. 2016, *A&A*, 585, A43
 Ciesla, L., Charmandaris, V., Georgakakis, A., et al. 2015, *A&A*, 576, A10
 Conley, A., Cooray, A., Vieira, J. D., et al. 2011, *ApJL*, 732, L35
 Cutri, R. M., Wright, E. L., Conrow, T., et al. 2014, *yCat*, 2328, 0
 da Cunha, E., Charlot, S., & Elbaz, D. 2008, *MNRAS*, 388, 1595
 da Cunha, E., Eminian, C., Charlot, S., & Blaizot, J. 2010, *MNRAS*, 403, 1894
 da Cunha, E., Walter, F., Smail, I. R., et al. 2015, *ApJ*, 806, 110
 Dale, D. A., Helou, G., Magdis, G. E., et al. 2014, *ApJ*, 784, 83
 Dey, A., Soifer, B. T., Desai, V., et al. 2008, *ApJ*, 677, 943
 Draine, B. T. 2003, *ARA&A*, 41, 241
 Draine, B. T. 2006, *ApJ*, 636, 1114
 Dunne, L., Eales, S., Edmunds, M., et al. 2000, *MNRAS*, 315, 115
 Eisenhardt, P. R. M., Wu, J., Tsai, C.-W., et al. 2012, *ApJ*, 755, 173
 Fan, L., Gao, Y., Knudsen, K. K., & Shu, X. 2018, *ApJ*, 854, 157
 Fan, L., Han, Y., Nikutta, R., Drouart, G., & Knudsen, K. K. 2016, *ApJ*, 823, 107
 Fritz, J., Franceschini, A., & Hatziminaoglou, E. 2006, *MNRAS*, 366, 767
 Genzel, R., Tacconi, L. J., Lutz, D., et al. 2015, *ApJ*, 800, 20
 Gruppioni, C., Pozzi, F., Rodighiero, G., et al. 2013, *MNRAS*, 432, 23
 Harper, D. A., Runyan, M. C., Dowell, C. D., et al. 2018, *JAI*, 7, 1840008
 Hjorth, J., Gall, C., & Michałowski, M. J. 2014, *ApJL*, 782, L23
 Ho, P. T. P., Moran, J. M., & Lo, K. Y. 2004, *ApJL*, 616, L1
 Holland, W. S., Bintley, D., Chapin, E. L., et al. 2013, *MNRAS*, 430, 2513
 Hopkins, P. F., Hernquist, L., Cox, T. J., & Kereš, D. 2008, *ApJS*, 175, 356
 Hwang, H. S., Elbaz, D., Magdis, G., et al. 2010, *MNRAS*, 409, 75
 Inoue, A. K. 2011, *MNRAS*, 415, 2920

- Kovács, A., Chapman, S. C., Dowell, C. D., et al. 2006, *ApJ*, 650, 592
- Landsman, W. B. 1993, in ASP Conf. Ser. 52, *Astronomical Data Analysis Software and Systems II*, ed. R. J. Hanisch, R. J. V. Brissenden, & J. Barnes (San Francisco, CA: ASP), 246
- Liang, L., Feldmann, R., Kereš, D., et al. 2019, *MNRAS*, 489, 1397
- Lianou, S., Barmby, P., Mosenkov, A., et al. 2019, *A&A*, 631, 38
- Magdis, G. E., Daddi, E., Béthermin, M., et al. 2012, *ApJ*, 760, 6
- Magnelli, B., Lutz, D., Saintonge, A., et al. 2014, *A&A*, 561, A86
- Mamajek, E. E., Prsa, A., Torres, G., et al. 2015, arXiv:1510.07674
- McMullin, J. P., Waters, B., Schiebel, D., Young, W., & Golap, K. 2007, in ASP Conf. Ser. 376, *Astronomical Data Analysis Software and Systems XVI*, ed. R. A. Shaw, F. Hill, & D. J. Bell (San Francisco, CA: ASP), 127
- Melbourne, J., Soifer, B., Desai, V., et al. 2012, *AJ*, 143, 125
- Narayanan, D., Dey, A., Hayward, C. C., et al. 2010, *MNRAS*, 407, 1701
- Noboriguchi, A., Nagao, T., Toba, Y., et al. 2019, *ApJ*, 876, 132
- Noll, S., Burgarella, D., Giovannoli, E., et al. 2009, *A&A*, 507, 3
- Pei, Y. C. 1992, *ApJ*, 395, 130
- Ricci, C., Bauer, F. E., Treister, E., et al. 2017, *MNRAS*, 468, 1273
- Rovilos, E., Georgantopoulos, I., Akylas, A., et al. 2014, *MNRAS*, 438, 494
- Rowan-Robinson, M. 2000, *MNRAS*, 316, 885
- Rowan-Robinson, M., & Wang, L. 2010, *MNRAS*, 406, 720
- Sanders, D. B., & Mirabel, I. F. 1996, *ARA&A*, 34, 749
- Santini, P., Maiolino, R., Magnelli, B., et al. 2014, *A&A*, 562, A30
- Schreiber, C., Elbaz, D., Pannella, M., et al. 2018, *A&A*, 609, A30
- Swinbank, A. M., Simpson, J. M., Smail, I., et al. 2014, *MNRAS*, 438, 1267
- Temi, P., Hoffman, D., Ennico, K., & Le, J. 2018, *JAI*, 7, 1840011
- Toba, Y., Bae, H.-J., Nagao, T., et al. 2017a, *ApJ*, 850, 140
- Toba, Y., Komugi, S., Nagao, T., et al. 2017b, *ApJ*, 851, 98
- Toba, Y., & Nagao, T. 2016, *ApJ*, 820, 46
- Toba, Y., Nagao, T., Kajisawa, M., et al. 2017c, *ApJ*, 835, 36
- Toba, Y., Nagao, T., Strauss, M. A., et al. 2015, *PASJ*, 67, 86
- Toba, Y., Nagao, T., Wang, W.-H., et al. 2017d, *ApJ*, 840, 21
- Toba, Y., Ueda, J., Lim, C.-F., et al. 2018, *ApJ*, 857, 31
- Toba, Y., Ueda, Y., Matsuoka, K., et al. 2019a, *MNRAS*, 484, 196
- Toba, Y., Yamada, S., Ueda, Y., et al. 2020, *ApJ*, 888, 8
- Toba, Y., Yamashita, T., Nagao, T., et al. 2019b, *ApJS*, 243, 15
- Tomczak, A. R., Quadri, R. F., Tran, K.-V. H., et al. 2016, *ApJ*, 817, 118
- Tsai, C.-W., Eisenhardt, P. R. M., Jun, H. D., et al. 2018, *ApJ*, 868, 15
- Tsai, C.-W., Eisenhardt, P. R. M., Wu, J., et al. 2015, *ApJ*, 805, 90
- Wilson, C. D., Rangwala, N., Glenn, J., et al. 2014, *ApJL*, 789, L36
- Wright, E. L., Eisenhardt, P. R. M., Mainzer, A. K., et al. 2010, *AJ*, 140, 1868
- Wu, J., Tsai, C.-W., Sayers, J., et al. 2012, *ApJ*, 756, 96
- Yang, M., Greve, T. R., Dowell, C. D., & Borys, C. 2007, *ApJ*, 660, 1198
- York, D. G., Adelman, J., Anderson, J. E., Jr., et al. 2000, *AJ*, 120, 1579